Effect of Antenna-Pointing Errors on Phase Stability and Interferometric Delay

P. W. Gorham[1] and D. J. Rochblatt[2]

We investigate the effects of Deep Space Network (DSN) antenna-pointing errors on the measured phase stability and interferometric delay. The results are based on point-source focal plane scans of various DSN antennas. These are combined with an analytical model to estimate the stability of the measured phase in the presence of time-varying errors in the pointing within the central lobe of the antenna beam.

The results suggest that phase fluctuations due to pointing errors are not yet a limiting factor in phase stability for 34-m antennas at frequencies below 12 GHz, but may become important at higher frequencies. For Cassini radio science measurements at 32 GHz (Ka-band), the need for closed-loop pointing control to meet the phase stability requirements is confirmed.

For very long baseline interferometry, the effective phase and group delay errors that result from the mutual pointing errors of two antennas are the important quantities. We have estimated the effects of pointing fluctuations on 2.3-/8.4-GHz (S-/X-band) delay and find that, under normal conditions, they are well below the limits imposed by uncertainty in the tropospheric delay. At higher frequencies, using large antennas, pointing-induced delay errors may become important under conditions of poor pointing stability.

I. Introduction

Antenna-pointing errors will affect the detected complex signal both in amplitude and phase, leading to a degradation of the detected signal power and to potential biases in the detected signal phase. The effects on signal amplitude are more easily treated. Models for the antenna focal-plane amplitude are straightforward to produce and verify since the focal-plane power is easily measured.[3]

Models for the focal-plane phase distribution must be produced using more complicated physical optics with a full treatment of diffraction and near-field effects. In addition, accurate focal-plane phase measurements are more difficult than amplitude measurements and often are subject to significant instrumental bias. This article combines physical-optics modeling for the focal-plane phase with measured

[1] Tracking Systems and Applications Section.

[2] Communications Ground Systems Section.

[3] This was treated in much detail in S. Slobin, "Antenna Pointing Errors and Pointing Loss—Basic Statistical Concepts," JPL Interoffice Memorandum (internal document), Jet Propulsion Laboratory, Pasadena, California, December 1996.

distributions to perform a semiempirical analysis of the behavior of phase measurements in the presence of pointing fluctuations. The analysis is supported by recent improvements in the phase-measurement accuracy of antenna main beams through the JPL Microwave Antenna Holography Program.

A. Single-Antenna Measurements

For a typical antenna using Cassegrain or similar optics, the amplitude distribution is described very accurately by low-order Bessel function approximations. Unlike the amplitude, which falls off steeply as one moves radially from the center of the main beam, the phase is nearly constant within the main beam for an aberration-free antenna system. However, once the effects of aberrations are included, the phase response off the beam center is no longer constant, and pointing errors will introduce errors in the measured phase.

The phase errors so introduced will affect single-antenna measurements by producing additional phase noise that will be correlated to the spectrum of antenna-pointing errors. Since the spectrum of pointing errors can have components extending to very low frequencies, the phase noise induced by these errors can become significant for the long-term phase stability of the measured signal. Long-term phase stability is critical to gravitational wave searches and other efforts based on measurements of satellite carrier phase with time. Thus, it is important to quantify this effect and its possible impact on these experiments.

B. VLBI

For very long baseline interferometry (VLBI) observations, the pointing errors of the individual antennas that form a baseline are presumed to be uncorrelated. Thus, the phase noise introduced in a very long baseline interferometer will depend on the differences of the phase errors due to the pointing errors. The standard interferometer observables include phase, phase rate, group delay, and delay rate.

We will show below that antenna aberrations of a fixed scale produce effects on the beam shape and phase that increase at higher frequencies. Thus, these two effects can conspire to produce a strong frequency dependence in the phase errors. Under such conditions, phase and group delay determined from dual-frequency interferometric observations (as in VLBI) can be affected if the phase errors are large enough or the radio frequency high enough.

In the following, we first make use of an analytical model to estimate the phase across the main beam by numerical integration of the appropriate equations. This integral is extended to include low-order aberrations of the antenna surface. We then apply the model to boresight scans of the amplitude and phase made on a number of Deep Space Network (DSN) antennas, validating the model and empirically deriving some estimates for the behavior of the phase errors with mispointing. From this, we then are able to construct, using an empirically constructed pointing time series, a prediction for Allan deviation at a number of wavelengths. Finally, for interferometry, we estimate the effects on the phase and group delay observables.

II. Analysis

Both parabolic and Cassegrain systems have been treated to estimate the on-axis field configurations [4,8]. Off-axis fields are treated in [12] and [2] and, to some extent, also in [4]. Here we combine results from [1], [4], and [11], in which an equivalent parabola formulation for treating the Cassegrain system is given. The equivalent parabola approach determines a prime-focus parabolic system that best approximates the response of a given Cassegrain antenna. This approximation will not provide insight into the effects of the subreflector on the telescope beam, but does allow a treatment of the system as a single-aperture diffraction problem and gives results that are in good agreement with actual Cassegrain measurements.

For the DSN antennas, we assume $f/D \sim 4$ for the equivalent parabola of the standard Cassegrain, which has a secondary/primary aperture ratio of 0.1–0.15 and a primary $f/D \sim 0.4$. The main limitations of the equivalent parabola approach are that it does not reproduce the larger focal plane curvature of the Cassegrain and that it introduces a larger degree of coma than is present in an actual Cassegrain. However, both of these effects are only important for off-axis analysis. Since we are concerned only with the region within the main beam, the equivalent parabola formulation is a good approximation.

The focal-plane fields for the parabola are estimated using the results of [1] for a spherically converging wavefront. For nearly on-axis measurements, a parabola can be thought of as a system for converting a plane wave to a converging spherical wave; thus, the approach in [1] is valid for our case. Born and Wolf also show that a small pointing error can be represented as a linear phase gradient (a phase tilt) across the reflector [1], which leads to a simple solution of the off-axis field for pointing errors within a few times of the telescope's beamwidth.

The complex field at position $\mathbf{r}$ is obtained by the Debye integral over the solid angle, Ω, of the aperture, A. The integral operates by transforming the aperture-plane phase distribution appropriate to a converging spherical wave to a focal-plane distribution:

$$E(\mathbf{r}) = \frac{-i}{\lambda} \int_A e^{i[k(\mathbf{q}\times\mathbf{r}')+\Phi(\mathbf{r}')+\theta]} d\Omega \tag{1}$$

where $\mathbf{r}'$ is the aperture-plane coordinate and $\mathbf{q}$ is the wave vector of the incident field. The integrand represents a plane-wave series that is a valid approximation to a collection of spherical wavelets, e^{ikr}/r (as given by the Huygens–Fresnel principle), for the region near the focus. For a discussion of how the Debye integral is constructed, see [1] and [2]. Aberrations, $\Phi(\mathbf{r}')$, or tilts, θ, enter as phase terms in the argument of the integral, which also is discussed in [1].

As one scans across the main beam of the focal-plane field that is represented by Eq. (1), the phase is found to be constant until the first null in the amplitude, where it jumps by $\pm\pi$. The amplitude is given by the classical annular aperture diffraction pattern (cf., the Jacobi–Bessel series expansion) modified somewhat by the effects of the subreflector support struts. However, in any real system, misalignment of optics and surface aberrations will induce phase distortion across the main beam, as discussed below.

A. Aberration Effects

Here we restrict our consideration to only the four primary Seidel aberrations: coma, astigmatism, spherical aberration, and distortion. In [1], Born and Wolf summarize the effects on the phase fronts associated with each of these aberrations. Coma can be ignored for the region within the main beam. Distortion requires a treatment that does not assume axial symmetry and complicates the analysis considerably. For simplicity, we have restricted ourselves here to the axially symmetric case; thus, we do not treat distortion directly. However, we have indirectly included distortion effects in an empirical fashion, as mentioned in the next section.

Astigmatism can be represented in Eq. (1) as

$$\Phi_A(\mathbf{r}) = kA\rho^2 \cos(2\psi) \tag{2}$$

where $k = 2\pi/\lambda$, A is a parameter that sets the magnitude of the aberration, $\rho = |\mathbf{r}|$, and ψ is the azimuthal angle around the aperture. It is a significant problem for radio antennas, which commonly are subject to gravity distortion. It produces a curvature in the phase that is different for elevation and azimuth.

Spherical aberration can be regarded as a curvature error, thus affecting the phase when the source phase center is radially moved from the optic axis, as in a pointing error. Following [1], it is represented in Eq. (1) as

$$\Phi_S(\mathbf{r}) = kB\rho^4 \tag{3}$$

where B again is the magnitude parameter, as above.

The aberrations are combined as

$$\Phi(\mathbf{r}) = \Phi_A(\mathbf{r}) + \Phi_S(\mathbf{r}) \tag{4}$$

in Eq. (1). This is accurate for deviations smaller than a wavelength, which we assume to be the case for these antennas. We have found empirically that these low-order aberrations are adequate to model the data at the level that we required in this study.

Since both of these aberrations are even functions, asymmetric distortion was not accounted for; in some cases presented here, such distortion is present. Figure 1 shows an example of results for a parabola equivalent to the Cassegrain systems considered here for four cases: no surface errors, and rms surface errors (consisting of a roughly equal mix of spherical aberration and astigmatism) of $\lambda/100$, $\lambda/30$, and $\lambda/15$.

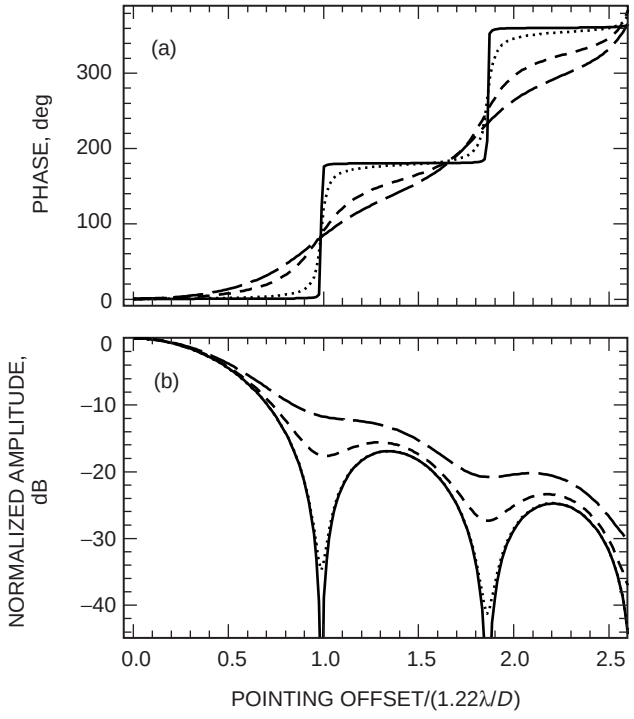

Fig. 1. Model phase and amplitude as a function of pointing offset for no surface aberrations (solid line), λ/100 rms (dotted line), λ/30 rms (short dashed line), and λ/15 rms (long dashed line): (a) phase and (b) amplitude.

B. Feed-Centering Errors

If the feed is displaced from the phase center of the antenna, where it was at the focus, the immediate result is a focus error, which will depend on the degree to which the displacement of the feed follows the focal-plane surface, which generally is hyperboloidal for a Cassegrain system. The resulting focus error appears to the first order in the phase and can be substantial. This is not strictly a pointing error, but will enter into the estimate of the pointing effects on the phase because, when the feed is not centered, each pointing offset introduces a different focus offset.

Modeling of the effects of off-center feeds is beyond the scope of this article, since it depends in detail on the shape of the off-axis focal-plane surface and produces a nonaxially symmetric effect, as in the case of distortion discussed above. We have not attempted to treat these effects analytically, but in one restricted case where it is evident that the results of such effects are present, we have included the effect empirically. This is the case where a linear phase gradient is apparent across the beam, and examples will be seen in the following section. In this case, the magnitude of the linear term has been estimated and included in the simulations that estimate Allan deviation.

III. Results

Figure 2 shows an example of a two-dimensional scan of the main beam of DSS 13, at a 12-deg elevation, using the Gstar4 geostationary satellite at 11.7 GHz. The contours show the log of the amplitude, and the phase is shown by the vector field. Zero degrees of phase is to the left, and the phase increases counterclockwise. The magnitude of the vectors also is scaled by the log of the amplitude. The heavy dashed circles show the nominal positions of the first null and second Airy maximum of the diffraction pattern. The global features of the phase behavior are shown here: the phase flip at the amplitude nulls as well as the first-order flatness of the phase across the central lobe.

Figure 3 shows the same data with an expanded scale to emphasize the main lobe. Both amplitude and phase can be seen to have some systematic variations that would not be present in a perfect system. Some of this may be due to the presence of the subreflector support struts, which can produce additional diffraction effects.

As the telescope points away from the source but still within the main beam, so that the main lobe moves off the phase center of the feed, the feed response will be affected by the shape of the phase front within the main beam. Since this shape is a complicated function of all of the effects mentioned here, we use here a semiempirical method, wherein the measured phase response will be used to constrain a model phase response that then will be used to estimate the phase stability. In practical terms, the coefficients A and B were varied until approximate agreement was reached over the portion of the phase within the main beam, providing a first-order estimate of the magnitude of the aberrations. As mentioned in the previous section, we also made a first-order estimate of the magnitude of any linear phase gradient that was apparent.

A. Main-Beam Scans

Figures 4 through 9 show scans of phase and amplitude for three DSN antennas: two 34-m beam-waveguide (BWG) antennas (DSS 25 and DSS 13) and one 70-m antenna (DSS 14), each for two elevations, 47 and 12 deg. These are representative scans, although the variations from scan to scan can be significant and can give phase and amplitude differences that are larger or smaller than shown. In each figure, numerical results using the Debye integral are shown, with phase and amplitude measurements taken at 11.7 GHz (2.56 cm) using the JPL Microwave Antenna Holography System (MAHST) [6]. The MAHST system employs a small reference antenna mounted alongside the antenna under test and uses beacon signals from Earth-orbiting satellites to produce high signal-to-noise (SNR) measurements of the complex antenna response in scans across the beam and also can be used to characterize the phase stability of the antenna with time.

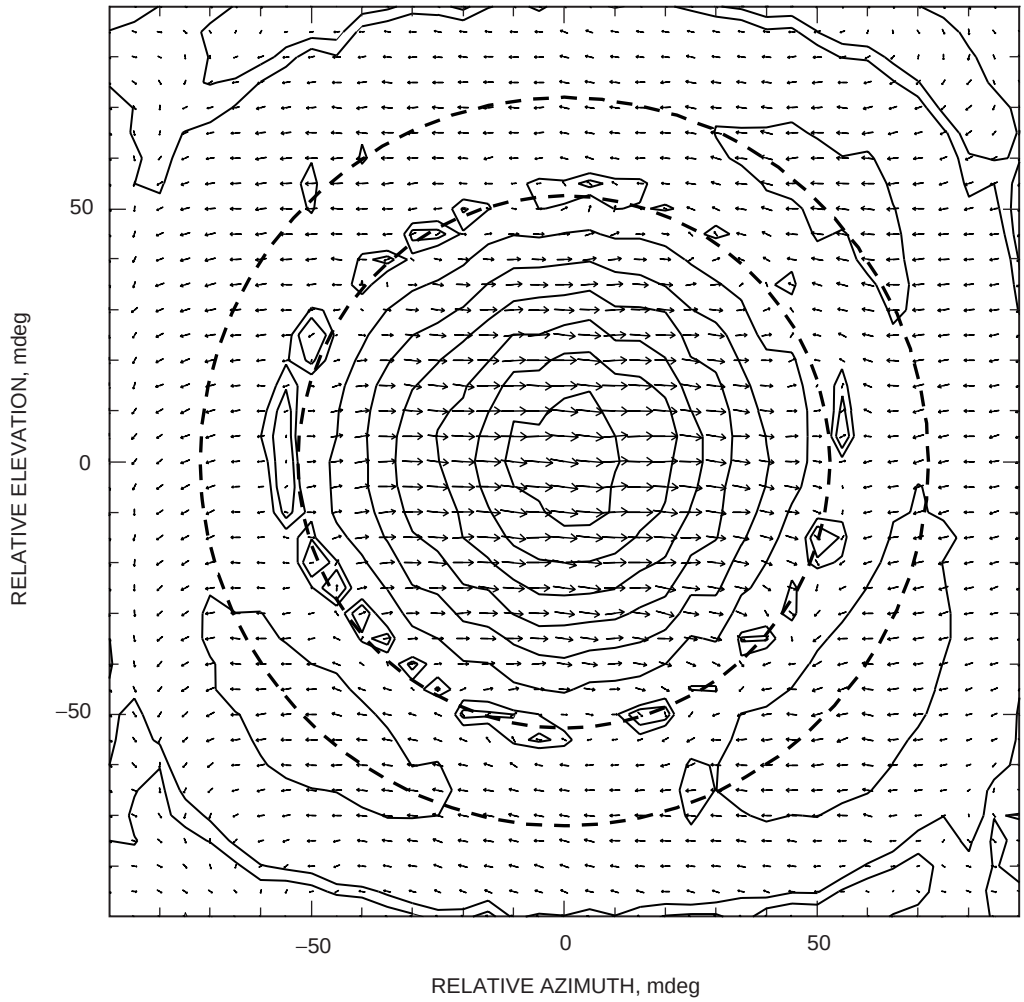

Fig. 2. A two-dimensional scan across the main beam of DSS 13 at 12-deg elevation. The contours show the amplitude, and the vector field shows the phase, with 0 deg to the right and phase increasing counterclockwise. The phase vectors also are scaled in length according to their respective amplitude. Contours are at 3, 4.5, 15, 30, 45, 60, 75, and 90 percent of the maximum amplitude. The statistical errors in both amplitude and phase are below 1 percent over the entire map. The heavy dashed circles show the positions of the first null and second maximum of the diffraction pattern.

1. DSS 25. The scans of DSS 25 at a 47-deg elevation show nearly ideal phase and amplitude distributions. The model shows good agreement for an rms spherical aberration of 0.25 mm across the aperture, consistent with holography measurements made with the MAHST [7] on the nearly identical DSS 24, which had an rms surface error of 0.25 mm after correction with the holography panel setting. At 12 deg, DSS 25 begins to show the effects of astigmatism, as expected from gravity loading. The model phase agreement is good over the main beam for an rms surface deviation of 0.35 mm, but the phase agreement near the first null is now poorer, indicating that higher-order aberrations or misalignments may be present. The amplitude agreement is reasonable even at the second maximum, however. For the purpose of this article, the goal was to get reasonable phase agreement only within the main beam.

2. DSS 13. DSS 13 is used at the BWG focus after transfer from the Cassegrain focus by a pair of off-axis ellipsoidal mirrors. Thus, the model may not account for some of the near-field effects of the transfer optics. At a 47-deg elevation, we see a possible effect of this in the differences between the azimuth and elevation scans. The azimuth scan shows excellent model agreement for a model rms surface

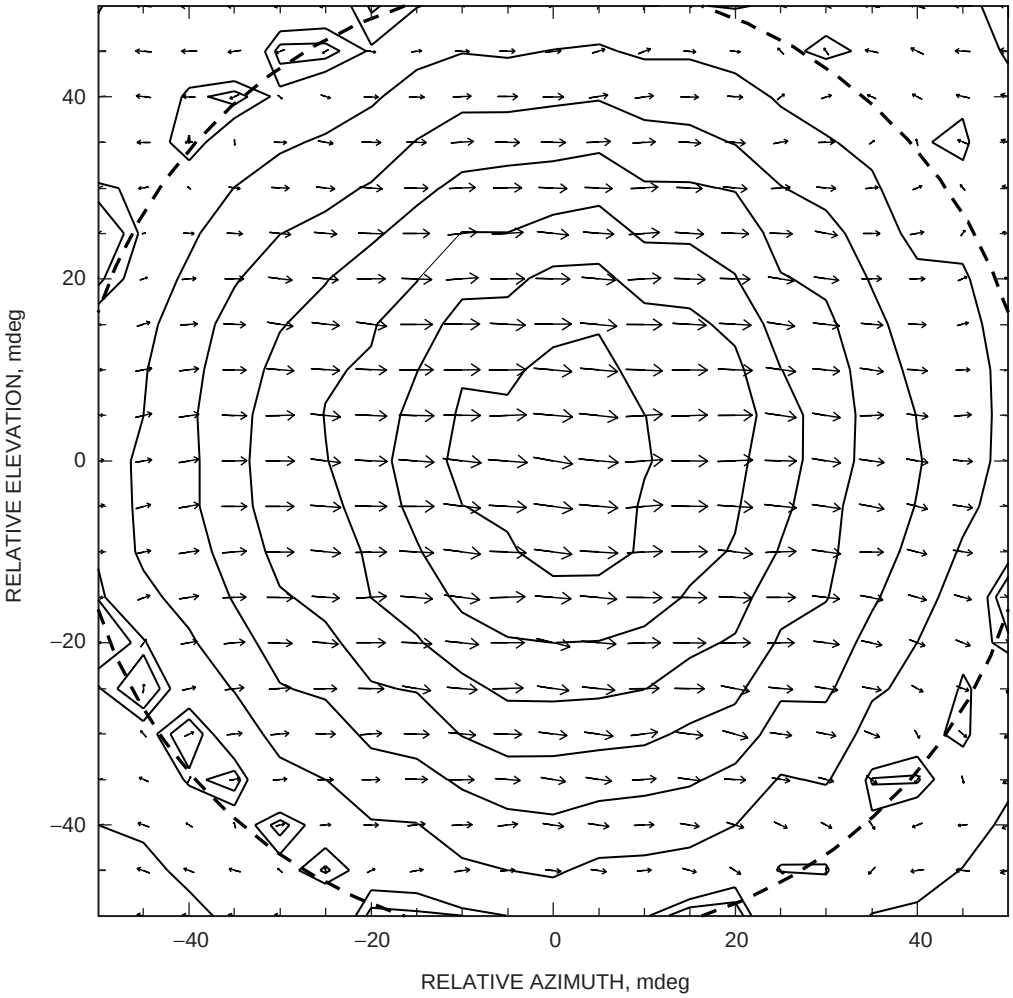

Fig. 3. The same as Fig. 2 except that the scale has been changed to emphasize the detail of the phase and amplitude in the main lobe. Contour levels are the same as in Fig. 2.

error of 0.3 mm, again consistent with the best results from antenna panel adjustment with the MAHST panel setting [6].

In contrast, the elevation scan shows asymmetric distortion (which the present model does not treat) with an effective amplitude of at least 0.55-mm rms if caused by antenna surface errors. However, such effects may be intrinsic to the BWG optics since an elevation scan necessarily moves across the long axis of the transfer ellipsoidal mirror, along which off-axis aberrations will be more pronounced. The first-order fitting employed here did not account for different aberration scales in azimuth and elevation, as are implied by these data. In this case, our simple aberration model is insufficient. However, to provide input to the analytical models, we use an rms of the implied aberrations in azimuth and elevation.

At a 12-deg elevation, DSS 13 now also shows probable effects of gravity astigmatism, with surface errors in both elevation and azimuth scans at the level of 0.55-mm rms, as predicted by the model phase.

3. DSS 14. DSS 14 is a 70-m antenna, with the scans made at the F1 focus. These scans show a greater level of surface aberrations, as expected. At a 47-deg elevation, the azimuth scan shows phase errors implying surface errors of ∼1-mm rms, confirmed by holography measurements. The elevation scan

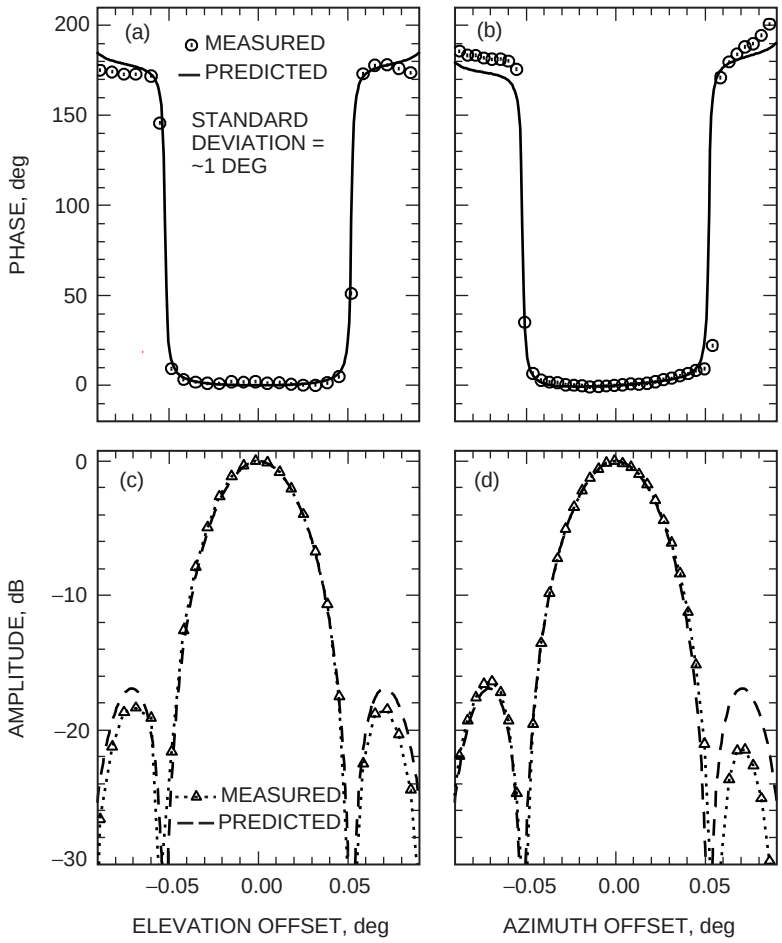

Fig. 4. Phase and amplitude across the main beam at 11.7 GHz for DSS 25 (34-m BWG antenna) at the F1 (Cassegrain) focus at a 47-deg elevation: (a) phase, elevation scan, (b) phase, azimuth scan, (c) amplitude, elevation scan, and (d) amplitude, azimuth scan. The model includes residual spherical aberration at the level of 0.25-mm rms and no astigmatism.

gives errors comparable to this value, also showing some asymmetric distortion. At 12 deg, the agreement with the model is only moderate for both azimuth and elevation taken together, with an implied rms surface distortion again of ∼1 mm.

B. Single-Dish Allan Deviation

We wish now to use this semiempirical model for the phase variations across the main beam to construct an estimate of the component of Allan deviation that would be produced as a result of the pointing-error-induced phase fluctuations. To do this, we require

(1) A way of constructing a realistic set of pointing fluctuations as a function of time for a given antenna,

(2) A model for the phase fluctuations produced by [1],

(3) An estimator for the Allan deviation, including a model for the sampling and how this enters the estimator.

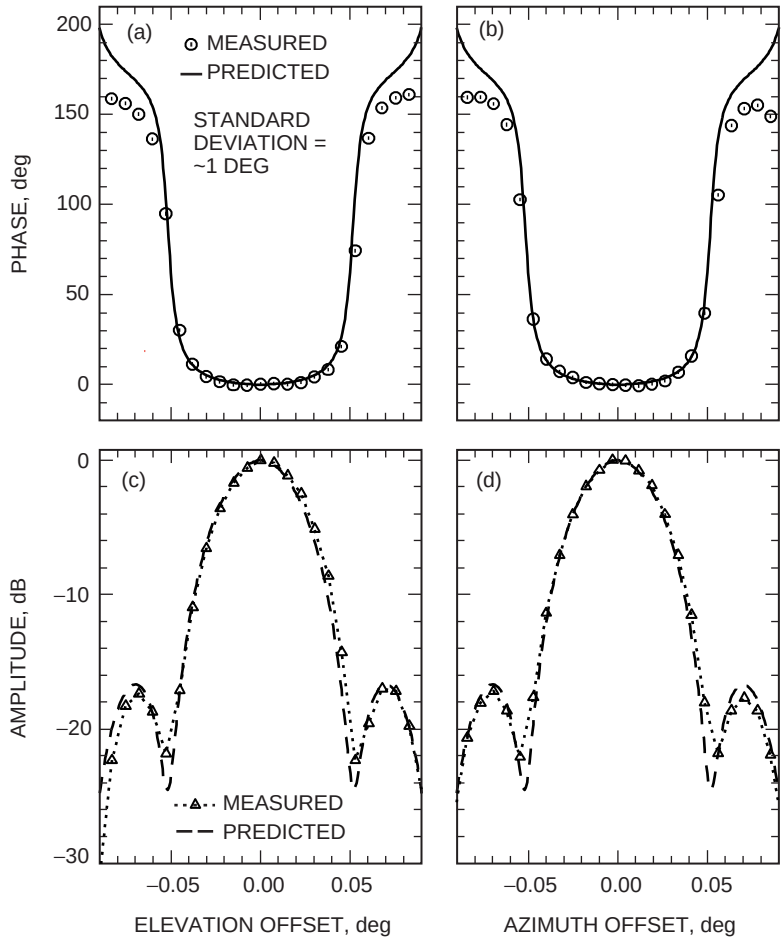

Fig. 5. Phase and amplitude across the main beam at 11.7 GHz for DSS 25 (34-m BWG antenna) at the F1 (Cassegrain) focus at a 12-deg elevation: (a) phase, elevation scan, (b) phase, azimuth scan, (c) amplitude, elevation scan, and (d) amplitude, azimuth scan. The rms surface error in the model is 0.35 mm.

The Allan variance is estimated for this random sequence of phase estimates by the prescription (cf., [10])

$$\sigma_y^2 = \frac{\langle (y_{k+1} - y_k)^2 \rangle}{2} \tag{5}$$

where

$$y_k = \frac{\phi(t_k + \tau) - \phi(t_k)}{2\pi\nu_0\tau} \tag{6}$$

Here τ is the averaging time (equal to the measurement time interval) for the phase samples, $\phi(t_k)$, and the brackets denote a time average over an ensemble of variance measurements.

A plausible pointing time series was constructed from phase measurements of a series of satellite tracks observed using an array feed system on DSS 13 that produces an estimate of the pointing error as

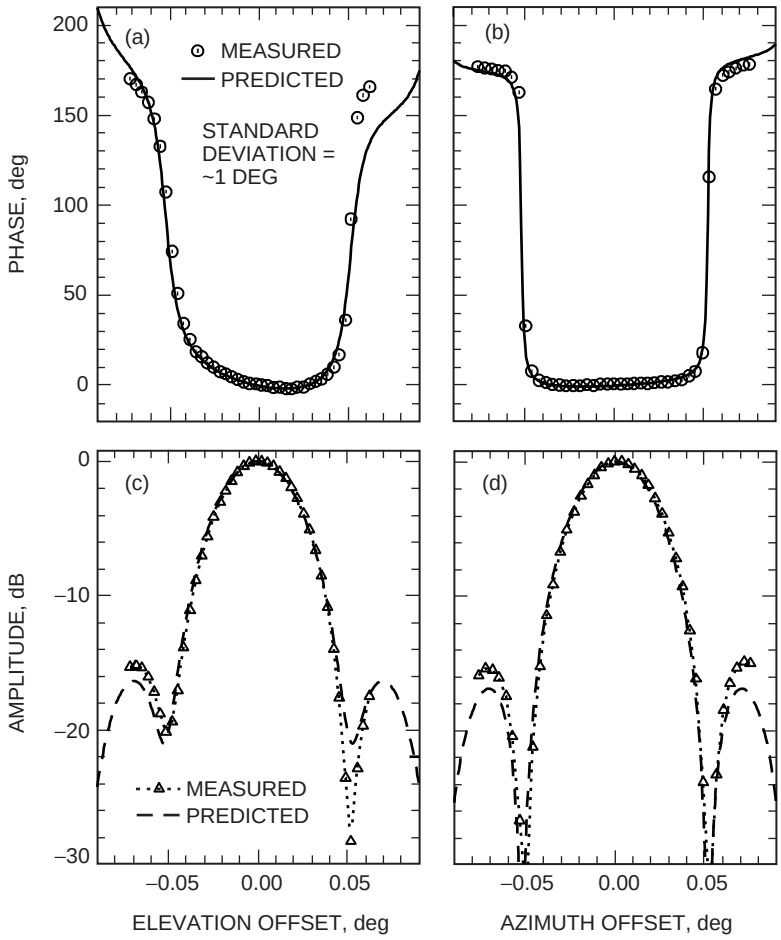

Fig. 6. Phase and amplitude across the main beam at 11.7 GHz for DSS 13 (34-m BWG antenna) at the F1 (Cassegrain) focus at a 47-deg elevation: (a) phase, elevation scan, (b) phase, azimuth scan, (c) amplitude, elevation scan, and (d) amplitude, azimuth scan. There is an rms surface error of 0.3 mm in azimuth and 0.55 mm in elevation.

a function of time, with precision of the order of 1 mdeg. A plot of one of these tracks is shown in Fig. 10, taken from a recent observation of the Mars Global Surveyor (MGS) spacecraft as it approached Mars.[4] This pointing time series was used as input to the phase estimation routines, which then produce a time series of observed signal phase fluctuations due to the pointing offsets. From this the Allan deviation is calculated, assuming that the integration time is equal to the averaging time at each time interval, τ.

Figures 11 through 13 show the estimated Allan deviation for the case where each antenna has the same pointing spectrum, modeled after that shown in Fig. 10. In each case, two curves are shown, one for Ka-band (32 GHz) and one for Ku-band (11.7 GHz). A fitted power law also is shown, and in each case the index is about -0.8. Since white phase noise should produce a power law index of -1, this indicates that there is some increased low-frequency power in the pointing spectrum.

In Fig. 11, we estimate the best-case Allan deviation for DSS 25, using the minimum level of aberrations observed, as at a 47-deg elevation. We also have simulated the case of elevations near 12 deg, and we find

[4] These data were made available by V. Vilnrotter and D. Fort, personal communication, Communications and Systems Research Section and Tracking Systems and Applications Section, Jet Propulsion Laboratory, Pasadena, California, 1997, and were taken as part of JPL's array-feed development program.

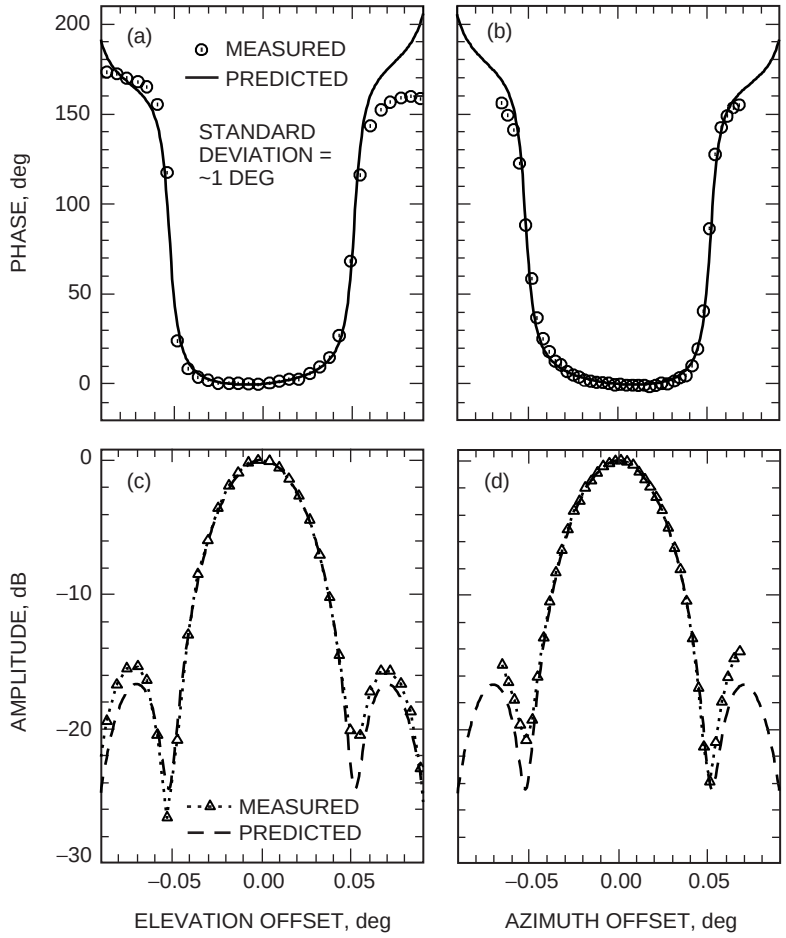

Fig. 7. Phase and amplitude across the main beam at 11.7 GHz for DSS 13 (34-m BWG antenna) at the F1 (Cassegrain) focus at a 12-deg elevation: (a) phase, elevation scan, (b) phase, azimuth scan, (c) amplitude, elevation scan, and (d) amplitude, azimuth scan. The rms surface error is 0.55 mm.

that the Allan deviation in this case is about 50 percent higher due to the increased antenna-aberration magnitude. For comparison, Fig. 11 shows values for the requirements and goals of the Ka-band Cassini gravity wave (GW) search. This will be discussed more in the following section. The stated requirements and goals used here and plotted in the figure are[5]

(1) Requirements:

$$\tau = 100 \text{ s} \quad \sigma_y(\tau) \leq 5 \times 10^{-15} \tag{7}$$

$$\tau = 1000 \text{ s} \quad \sigma_y(\tau) \leq 1.6 \times 10^{-15} \tag{8}$$

[5] R. Linfield, personal communication, Tracking Systems and Applications Section, Jet Propulsion Laboratory, Pasadena, California, 1997.

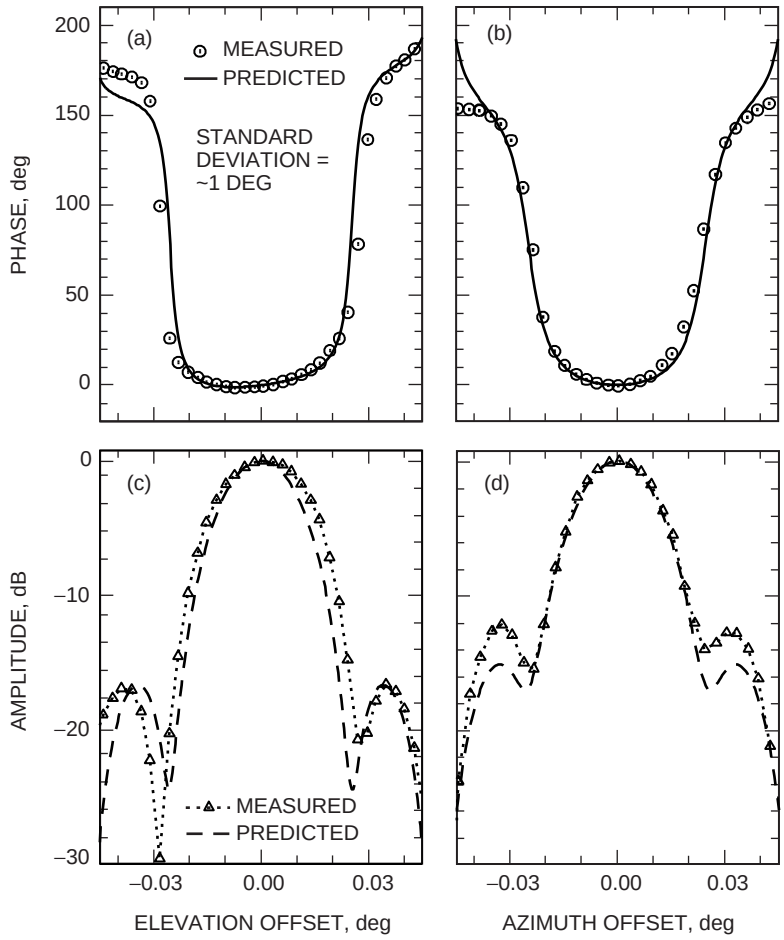

Fig. 8. Phase and amplitude across the main beam at 11.7 GHz for DSS 14 (70-m antenna) at the F1 (Cassegrain) focus at a 47-deg elevation: (a) phase, elevation scan, (b) phase, azimuth scan, (c) amplitude, elevation scan, and (d) amplitude, azimuth scan. The rms surface error in the model is ~1 mm.

(2) Goals:

$$\tau = 100 \text{ s} \quad \sigma_y(\tau) \leq 1.3 \times 10^{-15} \tag{9}$$

$$\tau = 1000 \text{ s} \quad \sigma_y(\tau) \leq 4 \times 10^{-16} \tag{10}$$

Figure 12 shows the result for DSS 13, which is applicable for most elevation angles since the rms surface deviation was found to be roughly constant with elevation, although the pattern may change. The Allan deviation is about a factor of 3 higher than that of DSS 25.

Figure 13 extends this analysis to a 70-m antenna, DSS 14, where we now have increased the mean-radial pointing error to about 7 mdeg, consistent with estimates we have made based on data obtained from the 70-m antennas.[6] We expect this level to be typical of the best pointing of these antennas

[6] The 70-m pointing data were made available by C. Jacobs, personal communication, Tracking Systems and Applications Section, Jet Propulsion Laboratory, Pasadena, California, 1997, and were taken as part of JPL's VLBI astrometry program.

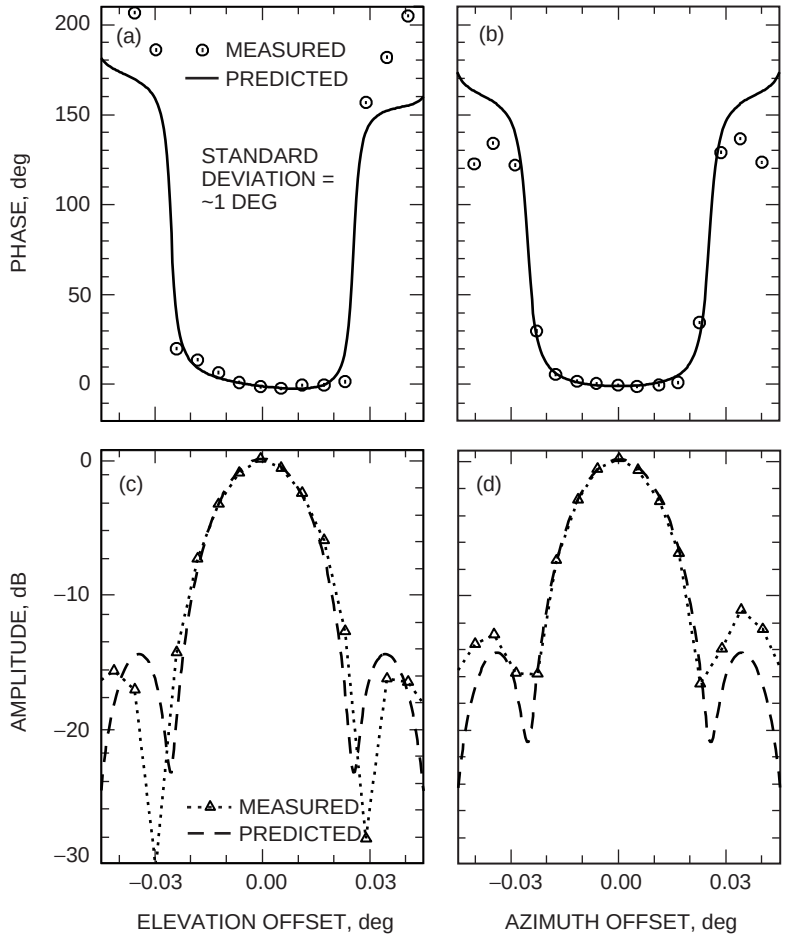

Fig. 9. Phase and amplitude across the main beam at 11.7 GHz for DSS 14 (70-m antenna) at the F1 (Cassegrain) focus at a 12-deg elevation: (a) phase, elevation scan, (b) phase, azimuth scan, (c) amplitude, elevation scan, and (d) amplitude, azimuth scan. The rms surface error is ~0.5 mm.

without some closed-loop pointing control. We include estimates of the Allan deviation at Ka-band, even though this antenna presently is not slated for Ka-band operation. Also plotted are estimates for X-band (8.4 GHz).

C. Comparison With Other Results.

We may compare these results with measured Allan deviations on DSS 25 taken from [5], using the MAHST system mentioned previously, at an elevation of 47 deg at Ku-band. Figure 14 reproduces the data from [5] with a τ^{-1} curve fitted to a portion of the data where it seems to best apply. This τ dependence is expected for the case where the noise is white phase noise, which may correspond physically to thermal noise in the receiver, for example. The lower curve shows the predicted Allan deviation that is due only to pointing effects as simulated here. The result suggests that the pointing noise contributes, at most, a few percent of the total Allan deviation in this measurement.

It is evident that the decrease in the measured Allan deviation with τ does not follow the expected τ^{-1} dependence for white phase noise, except over a limited averaging regime, between 10 to 100 seconds. The internal stability of the MAHST system is estimated to be 5.9×10^{-17}. Thus, both short- and long-term correlated phase noise are suggested by the data. The short-term noise likely is due to a combination of

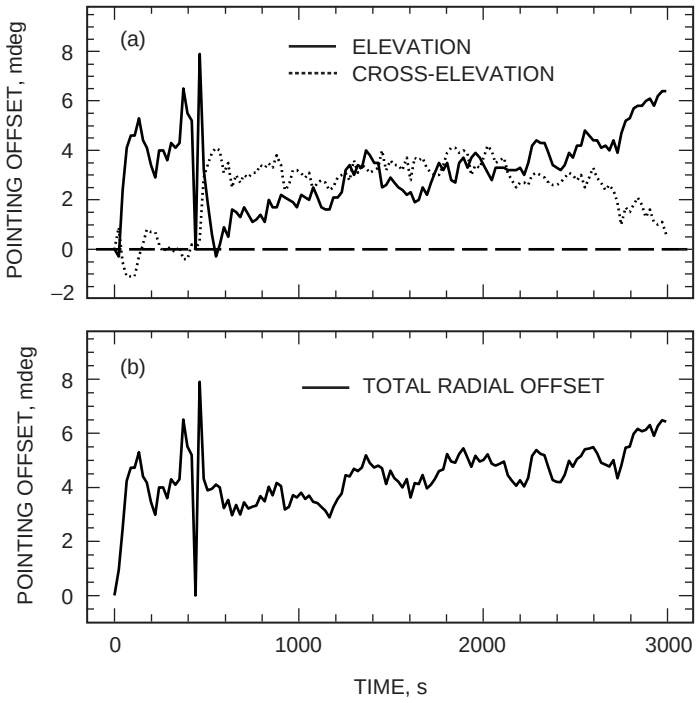

Fig. 10. A time series of cross-elevation, elevation, and radial pointing errors from a track of MGS with DSS 13 using an array feed system: (a) elevation and cross-elevation versus time and (b) total radial pointing offset versus time.

vibration and mechanical instabilities, whereas the long-term variations probably are drift effects, since the satellite position shifts by several mdeg during the observation and was not synchronously tracked.

IV. Implications for the Ka-Band Cassini Gravity Wave Search

Since the Cassini gravity wave search most likely will employ a closed-loop pointing system using some type of pointing-sensitive feed, these analyses are not directly applicable if the performance of these systems lives up to expectations, giving submillidegree precision.

It is interesting to note, however, that in the absence of a closed-loop pointing system, the phase noise associated with the pointing fluctuations produces an Allan deviation that probably exceeds the specifications for Cassini goals of 100s and 1000s and is within about 25 percent of the requirements. Given the uncertainty in this simulation, it will be prudent to ensure that the pointing control is robust during the observations, in particular when the elevation angle is lower, since this is the region where pointing errors produce the higher level of phase fluctuations.

The measured data of Fig. 14 suggest that saturation of the long-term Allan deviation could be a problem, if the source of this saturation is not in fact the small-scale drift of the satellite position. Further observations are in progress to investigate this issue. We note that long-term drifts in the focus or in the phase center relative to the feed position also can produce phase errors that will affect the long-term Allan deviation, and future efforts should investigate this as well.

V. Interferometric Delay Errors

We conclude with a short section on the effects of pointing errors on interferometric measurements of group delay observables, for example in VLBI. Here the issue is not the Allan variance of the phase,

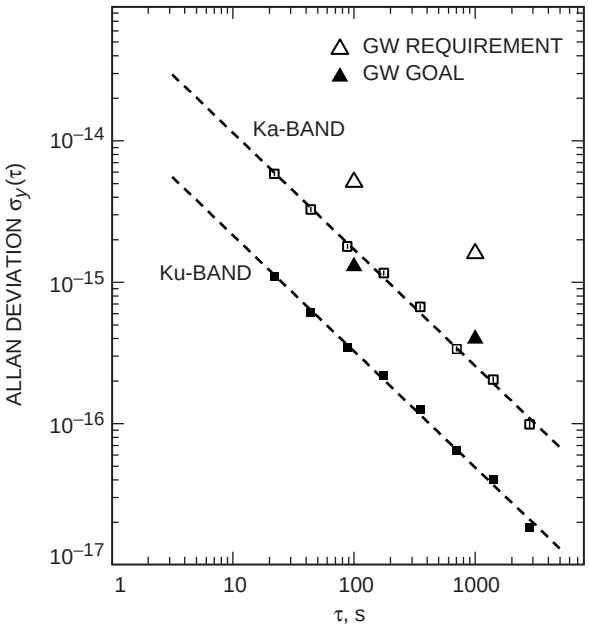

Fig. 11. Predicted Allan deviation for DSS 25 due only to pointing errors, using a model pointing time series constructed from measured pointing of DSS 13, with a mean radial pointing error of ~4 mdeg. The antenna elevation is assumed to be relatively high; thus, the rms surface errors are ~0.25 mm. For comparison, also shown are values for the requirements and goals of the Ka-band Cassini gravity wave search.

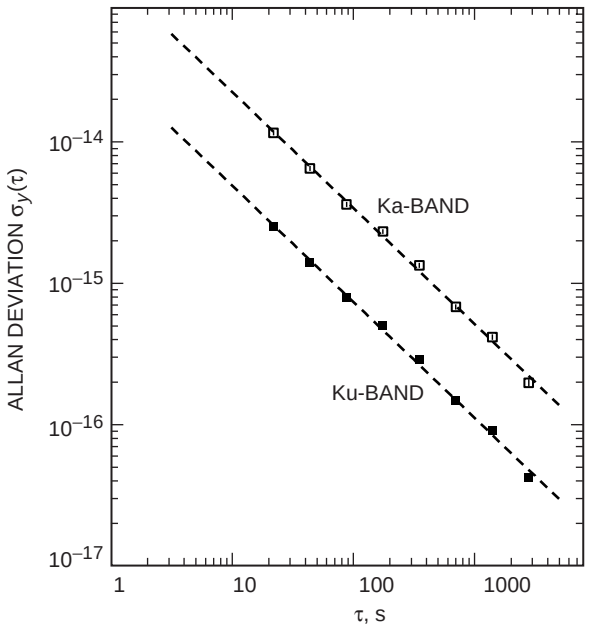

Fig. 12. Predicted Allan deviation for DSS 13 due only to pointing errors, using a model pointing time series constructed from measured pointing of DSS 13, with a mean radial pointing error of ~4 mdeg and an rms surface error of ~0.55 mm.

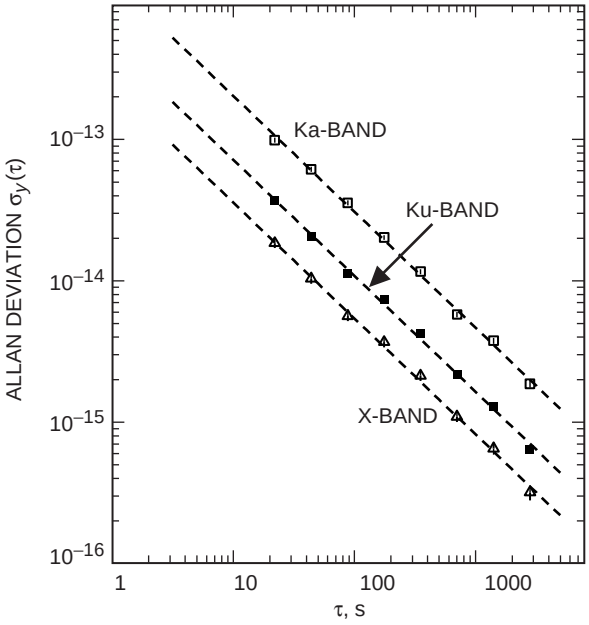

Fig. 13. Predicted Allan deviation for DSS 14 due only to pointing errors, using a model pointing time series constructed from measured pointing of DSS 13, with a mean radial pointing error of ~7 mdeg and rms surface errors of ~1 mm. Also shown are estimates for X-band.

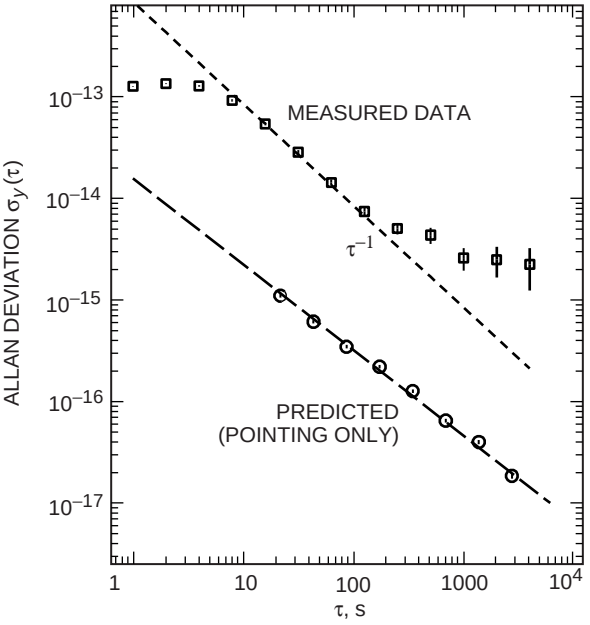

Fig. 14. A comparison of the measured Allan deviation for DSS 25 at 11.7 GHz and the best estimate of the pointing-error-induced component of the Allan deviation. The weather was clear and calm, and the antenna was performing static pointing at a stationary source at a 47-deg elevation.

but rather the equivalent group delay that would be observed in the presence of a frequency-dependent phase error.

A. Frequency Dependence

Figure 15 shows a plot of estimated radio-frequency dependence of the phase error for three fixed values of the pointing offset on a 34-m antenna with 0.55-mm rms surface error, using the model developed here. It is evident that the frequency dependence is at least proportional to ν^2 for any significant radial pointing offset, and the dependence is steeper for larger offsets, due to the fact that the phase error grows more than quadratically as it begins to approach the phase transition near the first amplitude null.

We note that the increase in the phase error with radio frequency as shown here is perhaps stronger than might be expected. This is due to two effects acting in the same direction. First, the size of the main beam is determined by the ratio λ/D, which decreases with increasing radio frequency, thus making the same mean radial pointing error more significant in terms of its fraction of the main beam. Second, for a fixed aberration magnitude, the ratio of the wavelength to the aberration also decreases with radio frequency, and, thus, the phase error increases proportionally. Since these two effects are multiplicative, we expect at least a ν^2 dependence, as observed. The additional steepening of the power law at higher frequencies is due to the fact that the phase errors become more pronounced as the radial pointing error approaches the edge of the beam.

B. Interferometric Phase Delay and Group Delay Errors

For a pair of antennas whose output signals are then cross-correlated to derive interferometric observables, we can assume that the individual antenna pointing errors are uncorrelated. Then the resulting phase error will depend on the mean difference in the individual phase errors at each antenna, which will,

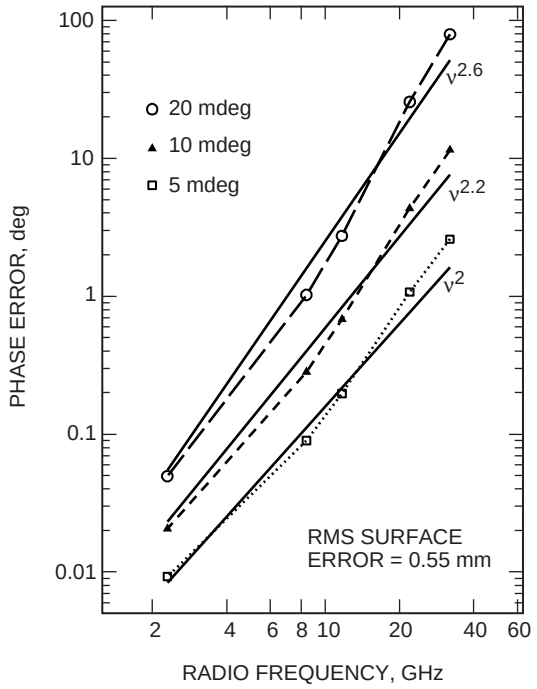

Fig. 15. Predicted radio-frequency dependence of the phase error for a 34-m antenna for three fixed values of the pointing offset. Also shown for comparison are power-law curves in radio frequency ν.

in general, be larger than the mean of phase errors at the individual antennas. Given the approximate ν^2 dependence apparent here, we can draw some initial conclusions concerning the behavior of the phase and group delay.

If we write the phase as power law in frequency ν,

$$\Phi(\nu) = \kappa\nu^{\alpha} \tag{11}$$

for some scale factor κ, then the phase delay is given by

$$\tau_{\Phi} = \frac{1}{2\pi}\frac{\Phi}{\nu} = \frac{1}{2\pi}\kappa\nu^{\alpha-1} \tag{12}$$

The group delay is determined from

$$\tau_g = \frac{1}{2\pi}\frac{\partial\Phi}{\partial\nu} = \frac{1}{2\pi}\alpha\kappa\nu^{\alpha-1} = \alpha\tau_{\Phi} \tag{13}$$

Since $\alpha \geq 2$ for phase errors induced from pointing errors, the resulting group delay effect will be at least twice that of the phase delay:

$$\tau_g(\nu) \geq 2\tau_{\Phi}(\nu) \tag{14}$$

In each of the following cases, the effect was modeled by assuming both antennas on the interferometer baseline have the same mean radial pointing error and that both have the same aperture size. Since VLBI measurements typically are averages over several minutes of 1- to 2-s phase samples, we have averaged over several hundred samples for each value of the mean radial error. Since the pointing time series were not available with sample times less than ∼20 s, we simulated a white noise pointing spectrum for shorter time intervals, with a magnitude that conformed to a given radial pointing error.

Each sample phase in the simulation is the difference between two random pointing-induced phases at each of the antennas, and these averages are computed for the two observing frequencies. The phase at each wavelength is scaled to an effective delay, and the delay difference at the two wavelengths is the observed delay error. Note that the delay error as determined in this manner must represent the worst case, since, in practice, a linear phase or group delay term is fitted for and calibrated out in typical astrometric VLBI data reduction (cf., [3]). As Lowe has shown, only the nonlinear residual of the pointing-induced error will affect the measured group or phase delay under the best circumstances, and in certain cases, errors of this form can be absorbed in part into fitted clock parameters, to which the delay is less sensitive [9]. The present result, therefore, should be taken as a *conservative* estimate of the effect of pointing-induced delay errors, and this consideration applies to all of the following analysis as well.

1. Phase-Connected Observations. For dual-frequency observations, such as the S-/X-band observations commonly used in VLBI, it sometimes is possible to estimate the phase delay with sufficient accuracy that phase connection is possible between the bands. Figure 16 shows the effect of pointing errors on the phase delay estimate. It is evident from this result that, for all reasonable values of the mean radial error (MRE), the phase delay is entirely negligible for the 34-m antenna, DSS 13. For example, at an MRE of 5 mdeg, typical under normal conditions, the S-/X-band phase delay error is less than 0.1 ps. Since state-of-the-art S-/X-band VLBI can achieve delay precision of only 10 ps or so, the pointing-error contribution under these conditions can be ignored. Under conditions of poor pointing stability and with

the use of 70-m antennas, S-/X-band phase delay errors may approach the 10-ps level, and under these conditions, the analysis must account for the pointing errors if phase connection is to be performed.

2. Effects on Group Delay Observables. Since phase connection is not often done for long baselines, because of the difficulties with atmospheric calibration, the effect of pointing errors on the group delay observables within a band is the relevant issue for most interferometric observations. Figure 17 shows the results for X-band group delay (which shows a larger effect than S-band because of the larger bandwidth). Again the effect is negligible for normal levels of pointing error, but may be marginally important under conditions when the pointing stability is poor or the antennas used are large.

VI. Conclusions

We have investigated in a variety of ways the effects of small pointing errors on the measured phase of an antenna signal. First, we have looked at the distribution of phase values over the main beam and their variation with different levels of antenna surface aberration. We have found that physical-optics modeling can adequately describe measured phase values on typical DSN antennas, and that the results are consistent with first-order estimates of the level of surface aberration present for a given antenna.

Second, we have applied these models to estimates of the behavior of an ensemble of phase measurements made at a single dish. Using existing data to constrain the model and provide input parameters and time series, we have estimated the level of Allan deviation due only to pointing errors that is likely to be present for measurements made at typical DSN antennas under typical operating conditions. Comparison of these estimates with actual Allan deviation measurements in one case suggests that the pointing contribution to the Allan deviation is of the order of a few percent of the total in this particular case. We also considered the effect of pointing-error induced Allan deviation at DSS 25 on the Cassini gravity wave goals and requirements if the pointing were not under closed-loop control, and we find that pointing-induced phase errors could be an important limitation in this case.

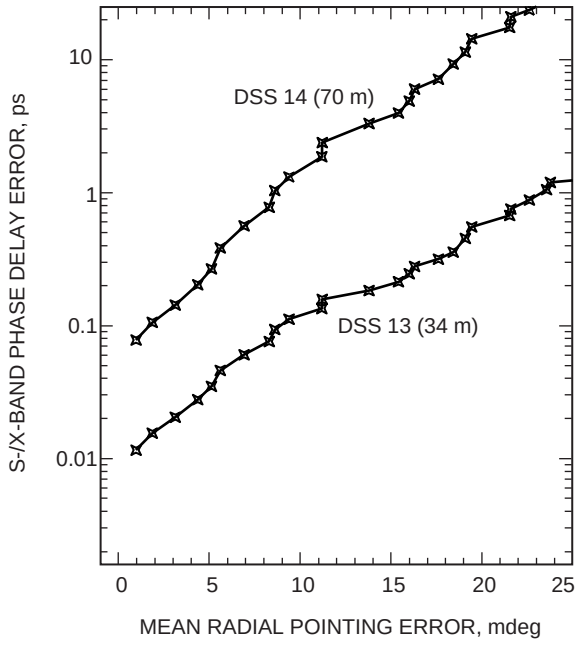

Fig. 16. Predicted group delay error for S-/X-band interferometric observations with two antennas (70-m and 34-m) and phase distributions similar to those in Figs. 7 and 8.

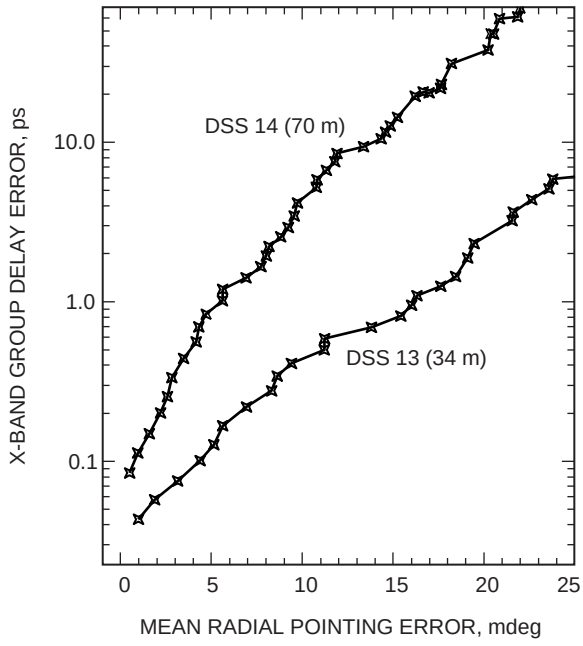

Fig. 17. Predicted group delay error for X-band interferometric observations with two antennas (70-m and 34-m) and phase distributions similar to those in Figs. 7 and 8.

Finally, we have considered the effect of such phase errors on VLBI observables and found that they are likely to be at least an order of magnitude below the present limitations imposed by tropospheric calibration uncertainties and are, thus, negligible at present.

Acknowledgments

Thanks to C. Jacobs, R. Linfield, S. Lowe, and G. Resch for useful comments and insight; V. Vilnrotter and D. Fort for the use of their array feed data for the pointing time series; and D. Rogstad for use of computer resources for a large part of this analysis.

References

[1] M. Born and E. Wolf, *Principles of Optics*, Oxford: Pergamon, 1959.

[2] J. D. Jackson, *Classical Electrodynamics*, Chapter 9, New York: Wiley and Sons, 1962.

[3] S. T. Lowe, *Theory of Post-Block II VLBI Observable Extraction*, JPL Publication 92-7, Jet Propulsion Laboratory, Pasadena, California, 1992.

[4] H. C. Minnett and B. E. Thomas, "Fields in the Image Space of Symmetrical Focussing Reflectors," *Proc. IEE*, vol. 115, no. 10, pp. 1419–1430, 1968.

[5] D. J. Rochblatt, P. H. Richter, and T. Otoshi, "A Microwave Performance Calibration System for NASA's Deep Space Network Antennas, Part 2: Holography, Alignment and Frequency Stability," *Proceedings of the 10th International Conference on Antennas and Propagation*, vol. 1, pp. 1.150–1.155, April 1997.

[6] D. J. Rochblatt and B. L. Seidel, "Microwave Antenna Holography," *IEEE Trans. Micr. Theory and Techn.*, vol. 40, no. 6, pp. 1294–1300, 1992.

[7] D. J. Rochblatt, P. M. Withington, and H. J. Jackson, "DSS-24 Microwave Holography Measurements," *The Telecommunications and Data Acquisition Progress Report 42-121, January–March 1995*, Jet Propulsion Laboratory, Pasadena, California, pp. 252–270, May 15, 1995.
http://tda.jpl.nasa.gov/tda/progress_report/42-121/121A.pdf

[8] W. V. T. Rusch, "Scattering From a Hyperboloidal Reflector in a Cassegrain Feed System," *IEEE Trans. Antenna Prop.*, vol. AP-11, pp. 414–421, 1963.

[9] O. J. Sovers, J. L. Fanselow, and C. S. Jacobs, "VLBI: Theory, Results and Future," *Rev. Mod. Phys.*, in press, to appear in vol. 70, no. 4, October 1998.

[10] A. Thompson, J. Moran, and G. Swenson, Jr., *Interferometry and Synthesis in Radio Astronomy*, New York: Wiley and Sons, 1986.

[11] W. C. Wong, "On the Equivalent Parabola Technique to Predict the Performance Characteristics of a Cassegrainian System With an Offset Feed," *IEEE Trans. Antenna Prop.*, vol. AP-21, pp. 335–339, 1973.

[12] W. H. Watson, "The Field Distribution in the Focal Plane of a Paraboloidal Reflector," *IEEE Trans. Antenna Prop.*, vol. AP-12, pp. 561–569, 1964.